5 DEVELOPMENT OF AN ELECTROCATALYTIC HYDROCARBON C-H FUNCTIONALIZATION SYSTEM USING TRAPPED FERRATE ANION (FeO_4^{2-}) ACTIVE SITES

5.1. Overview

Here, we change focus slightly from solar fuels to solar materials. Ethylene (C_2H_4) and ammonia (NH_3) are the two most energy-intensive materials produced on the planet. We believe, since they are the products of reduction of CO_2 and N_2, that they could be coupled into our solar water oxidation scheme. The electrons and protons needed to produce these highly value-added materials then would come from water, and the massive amount of energy currently used in their production would come from sunlight.

We wanted to determine the stability of our [NiFe]-LDH water oxidation catalyst in the presence of various hydrocarbon feedstocks, and we were surprised to find that the catalyst was able to *directly oxidize many C-H bonds with regioselectivity.* This chapter is dedicated to our preliminary work in this area, but much of this territory remains uncharted. The final sections are presented more as proposed research which we intend to complete in the near future.

5.2. Significance

The *selective*, catalytic activation of carbon-hydrogen bonds in simple hydrocarbons remains a significant challenge in organic chemistry. Despite marked progress over the previous decades, a general means of selectively oxidizing Csp3-H bonds using earth-abundant catalysts remains elusive to synthetic chemists. Herein we propose an electrocatalytic approach to selective C–H oxidation reactions of simple hydrocarbons through the repurposing of an earth-abundant water oxidation catalyst with a ferrate-like active site. This proposal is supported by preliminary data on the selective reaction of some simple hydrocarbons, including methane. Importantly, the selectivity of this catalyst is tuned by

modulating the applied potential, providing a unique means of control for this reaction. We initially aim to develop these preliminary hydrocarbon C–H oxidation results via exploration of both substrate tolerance and mechanism. Following this, we hope to extend this approach to other C–H functionalization reactions, such as the synthetically-relevant problem of C–H fluorination.

The importance of C–H functionalization for the field of organic synthesis is largely accepted by modern chemists, with the selective transformation of unactivated C–H bonds into other functional groups being viewed as a "holy grail" of chemical reactivity.[1-3] The reason for this is obvious: if selective C–H functionalization of simple hydrocarbons was possible and easy, the means of synthesizing almost any geometrically-possible molecule could be within reach.[4-6] Csp3–H bonds (e.g. in methane) are particularly difficult in this regard, positioning their selective functionalization as a preeminent challenge in C–H activation studies.

From the plethora of important studies detailing selective Csp3-H functionalization, several general strategies have emerged. The first approach, electrophilic activation, stems from Shilov's seminal studies with aqueous platinum chemistry.[7] Later, Bergman[8] and Graham[9] reported the basis for the second major class of activation processes: oxidative addition. Studies of d^0 metals have shown sigma-metathesis[10] to proceed readily under mild conditions and, finally, increased understanding of biological C–H functionalization reactions has revealed non-organometallic[11] C–H Activation (NOCHA) to be a highly relevant and general means of activating alkyl C–H bonds.

NOCHA comprises all processes wherein a proton and one or more electron are removed from an organic substrate in one or more steps to generate discrete, uncoordinated intermediate(s), often synthetically-versatile[12] radicals. Three subfamilies of this process are most common for the activation of Csp3–H bonds: electron transfer-proton transfer (ET-PT), proton-coupled electron transfer (PCET), and hydride transfer (HT). ET-PT is composed of two elementary steps: single electron transfer (SET) oxidation of the substrate to generate a radical cation intermediate followed by deprotonation to furnish a neutral radical (Figure 5.1a). PCET can be seen as a subset of ET-PT wherein the electron and proton move during

the same elementary step, allowing for a lower activation barrier than ET-PT in some situations (Figure 5.1b). A special case of PCET where the proton and electron transfer from the same starting orbital to the same ending orbital as a unit is called hydrogen atom transfer (HAT). HT can be seen as HAT with an extra electron, with the concerted departure of a hydride fragment generating a carbocationic intermediate (Figure 5.1c).

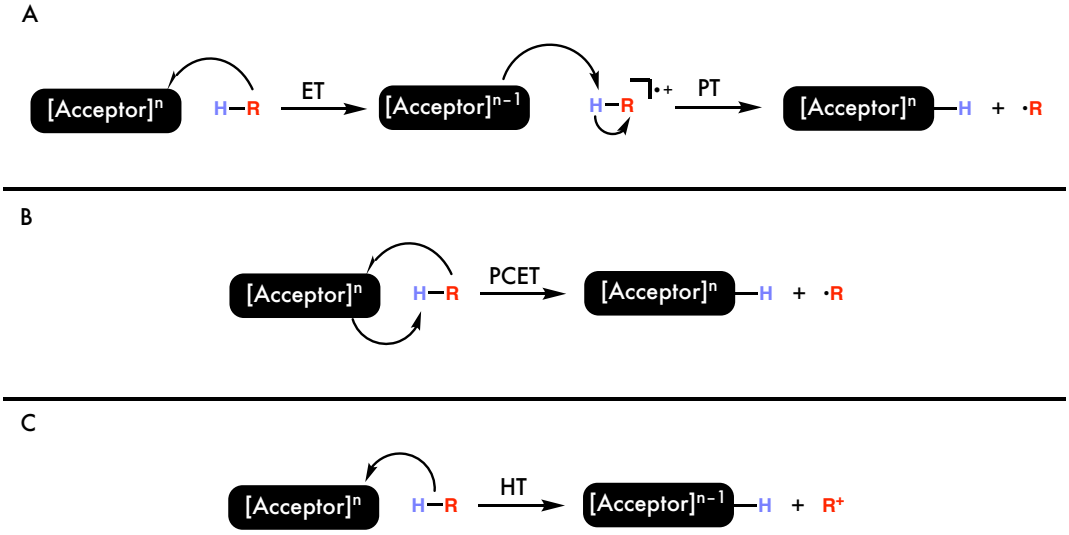

Figure 5.1. Schematic of the three non-organometallic C–H activation (NOCHA) processes relevant to Csp3–H functionalization: A) electron transfer-proton transfer (ETPT), B) proton-coupled electron transfer (PCET), and C) hydride transfer (HT). Figure reproduced with permission from Julian West.

Notably, these are common motifs in biology to functionalize unactivated C–H bonds,[13] particularly in the iron-dependent heme (e.g. P450) and non-heme enzymes.[14] These enzymes achieve C–H activation through high-valent iron-oxo species which are able to perform NOCHA outer-sphere reactions. Synthetic chemistry has been inspired by these systems, with both porphyrinoid[15,16] and non-heme[17-19] systems being devised to catalytically activate C–H. However, like their enzymatic congeners, these catalysts present several drawbacks. First is the relatively high complexity of the supporting ligands often required for reactivity, limiting the attainability of many desired catalytic frameworks. Second is the high specificity of each individual catalyst. This selectivity precludes tunability within a

single catalyst. Finally, these systems frequently decompose under reaction conditions, often through the oxidation of the ligand framework.

More robust organic oxidants include high-valent metal oxides, such as potassium permanganate ($KMnO_4$), manganese dioxide (MnO_2), chromium trioxide (CrO_3), potassium chromate (K_2CrO_4) and potassium dichromate ($K_2Cr_2O_7$).[20] The use of these reagents requires delicate control of reaction conditions to achieve reproducible results; often, competing side reactions (*e.g.* over-oxidation and acid/base chemistry) are overwhelming, especially in multistep syntheses. Furthermore, the regio- and stereospecificity is poor at elevated temperatures, limiting their utility in industrial settings. Finally, metal-based oxidants are often highly toxic; in particular, chromium and osmium are well-known carcinogens. The stoichiometric oxidation of an organic substrate often produces excessive amounts of contaminated waste.

All of the above-mentioned oxidative C–H functionalizations require stoichiometric reagents, whether strong oxidants (e.g. H_2O_2) or oxo-transfer reagents (e.g. iodosobenzene). While a terminal electron acceptor will always be required for a net-oxidative process, the possibility of using an abundant chemical species (e.g. atmospheric oxygen) would be of great interest. Recent reports from Gunnoe[21] and Baran[22] suggest that electrocatalysis may be a promising alternative to direct chemical transformations.

The development of a tunable, "green" oxidation catalyst that could be run electrochemically would be of great importance for the synthesis of pharmaceuticals and value-added chemicals. The annual worldwide production of potassium permanganate is estimated to be ~30,000 metric tons, most of which is used as an oxidant in industry.[23] Iron is both earth-abundant and environmentally benign, and the products of ferrate reduction are iron(III) oxides and hydroxides—rust.

5.3. Background

5.3.1. Ferrate

The tetrahedral[24] d^2 ferrate anion (FeO_4^{2-}) has been identified as a versatile and mild oxidant for organic substrates, similar in reactivity to permanganate (MnO_4^-). Although the syntheses of the sodium[25] and potassium[26] ferrate salts were first reported in 1951, relatively little is known about the reactivity and potential uses of ferrate.

Recent studies utilizing ferrate for waste water treatment,[27] and the identification of ferrate as a nominally homogeneous water oxidant[28] has generated renewed interest in the unusual, reactive species. Due to its relative ease of production and stability in air, potassium ferrate has been studied more extensively than the sodium, strontium, and barium salts.

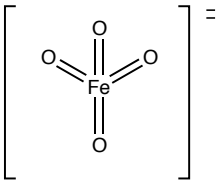

Figure 5.2. Bonding scheme for the ferrate dianion. The molecular geometry is tetrahedral.

The potassium salt is readily purified by precipitation of sodium ferrate in potassium hydroxide,[29] though a more recent technique involves the direct production of K_2FeO_4 from $Fe(NO_3)_3 \cdot 9H_2O$ in concentrated bleach.[30] Also of significant interest is the production of ferrate electrochemically, which features direct oxidation of an iron anode in saturated KOH.[31-33]

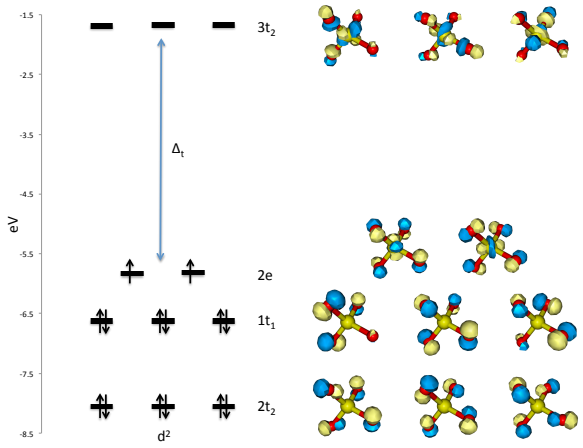

Figure 5.3. Calculated one-electron orbital levels for FeO_4^{2-} in the gas phase, showing LUMO, HOMO, HOMO-1 and HOMO-2 levels.

Güdel and coworkers have extensively studied the solid-state absorption and emission spectra of ferrate,[34-36] noting two sharp absorption features at 6209 and 9118 cm^{-1}. These are assigned to the spin-flip transitions within the e^2 manifold, namely $^3A_2 \rightarrow {}^1E$ and

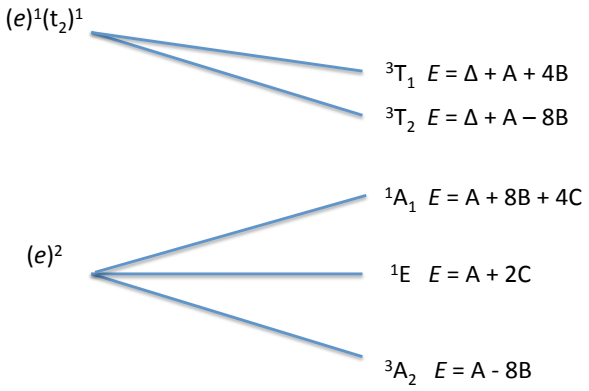

Figure 5.4. Strong-field splitting diagram for the lowest energy configurations. Matrix elements are given in terms of the Racah parameters.

$^3A_2 \rightarrow {}^1A_1$, respectively.

Although initial studies have not found that light plays a significant role in the reactivity of ferrate,[37] these excited states must be more oxidizing than the ground state by ca. 1 eV. This has led to our ongoing study of the photophysics of ferrate in an attempt to use light to promote and direct its reactivity.

The reactivity of ferrate with organic substrates is similar to that of permanganate (Figure 5.5), whereby primary and secondary alcohols and amines are converted to the corresponding aldehydes and ketones.[38] Darling et al. demonstrated regioselectivity, using ferrate to preferentially oxidize the primary alcohols in carbohydrates,[39] while Tsuda and Nakajima showed that the final product for benzyl alcohols is the corresponding aldehyde, rather than the carboxylic acid.[40] Sharma and coworkers have explored potential applications for pharmaceuticals and complex synthesis by the oxidation of sulfonamide antimicrobials, estrogens, endocrine disrupters and amino acids.[41] Recent reports indicate that $BaFeO_4$, in the presence of Lewis acids (*e.g.* $MgCl_2$, BF_3), oxidizes and chlorinates a variety of organic substrates at relatively high yields.[42]

Like potassium permanganate, the purple potassium ferrate powder remains stable in air for prolonged periods of time; in neutral or acidic conditions, however, the ferrate anion rapidly decomposes, evolving dioxygen and forming ferric hydroxide products. Aqueous stability is achieved at pH > 10, providing evidence that the protonated forms of ferrate are

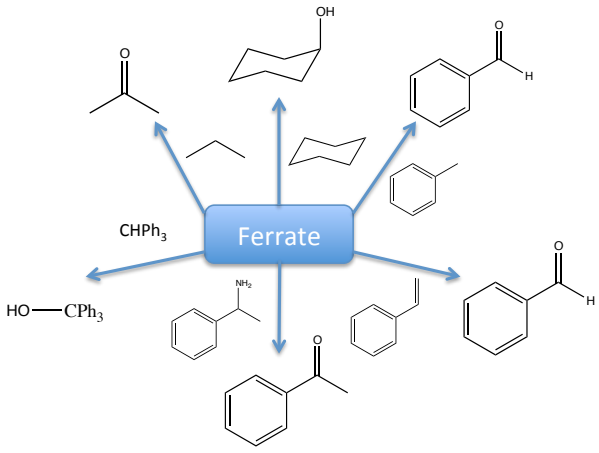

Figure 5.5. Examples of chemical oxidations by ferrate (FeO_4^{2-}).

the reactive species for water oxidation. The Fe(VI/III) reduction potential was calculated by calorimetric studies[43] for the reaction of K_2FeO_4 with $HClO_4$ and found to be 2.20 and 0.72 V versus NHE under acidic and basic conditions, respectively.[44] These values are significantly higher than the Mn(VII/IV) couple (1.679 V at pH 1, 0.588 V at pH 14), in agreement with the increased reactivity of ferrate. To date, no feasible catalytic pathway for ferrate oxidation has been proposed or developed.

At least two studies[30,44] have attempted to improve the regio- and stereoselectivity of ferrate oxidations by associating the potassium salt with microporous adsorbents

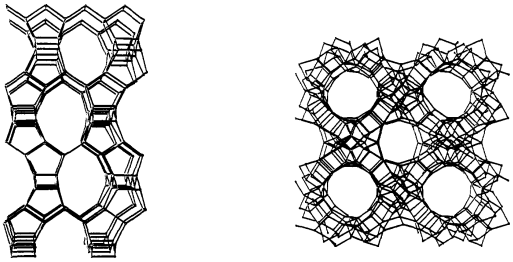

Figure 5.6. Stereoviews of the ZSM-5 zeolite framework. Reproduced from reference 24.

(aluminosilicates). Depending on the identity of the clay scaffold, yields for benzyl alcohol oxidation to benzaldehyde ranged from excellent (99%, K10 clay) to poor (1%, acidic alumina). These procedures have the primary benefit of being compatible with organic solvents, whereas potassium ferrate alone is generally insoluble. These clays have not been developed commercially (unlike those for lower-valent iron-adsorbed clays) because of the difficulty in purification of the ferrate-scaffold-product suspension. Permanganate, in contrast, has been successfully incorporated into a zeolite to produce a purely heterogeneous paradigm for organic oxidation.[45-47] Zeolites (Figure 5.6) have become attractive for catalysis over the past three decades owing to their shape discrimination, stability, ease of use, and potential for enantioselectivity.[48] The proposed work seeks to incorporate ferrate into "trapped" systems, much like the zeolite-permanganate model, and to develop a means of effecting electrocatalytic turnover for the system.

5.3.2. Thermodynamics of Ferrate Oxidations

Pulsed radiolysis studies have identified many of the intermediate products of ferrate oxidation, including the singly reduced FeO_4^{3-} species, which is a stronger oxidant than the iron(VI) species itself.[49] It is proposed that the iron(V) species is more substitutionally labile than proper ferrate, allowing substrate (*e.g.* H_2O_2) to bind to the metal center.[50] Studies of the decay kinetics of FeO_4^{3-} reveal rates in the free radical regime ($k \approx 10^7$ M^{-1} s^{-1}).[51] Additionally, the degree of protonation of the iron species is shown to be of critical importance, with the protonated forms ($HFeO_4^-$, H_2FeO_4) being the reactive species. The mechanism of stoichiometric water oxidation by ferrate at pH 1 has been probed by both stopped-flow experiments and DFT calculations.[52] Roth and coworkers propose a μ-oxo diferrate intermediate species, $[H_4Fe_2O_7]^{2+}$, with a structure similar to dichromate at low pH (Figure 5.7). They propose that O-O bond formation occurs by direct oxo-oxo coupling between neighboring iron centers, or by water attack on an electrophilic oxo. The mechanism at higher pH is less well understood, but is generally believed to be first-order in ferrate concentration with much slower rates ($k \approx 10$ M^{-1} s^{-1}), indicating an alternate mechanism is operative.[53]

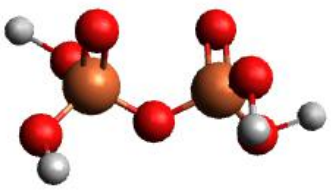

Figure 5.7. DFT-optimized structure of the proposed diferrate intermediate.

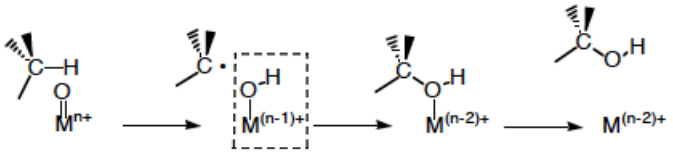

Figure 5.8. Rebound mechanism for metal-oxo C-H bond activation. The key O-H bond is indicated.

Considering the "trapped" nature of our ferrate mimics, we expect to favor a unimolecular mechanism inside the catalyst structure. Coupled with the strong pH dependence of ferrate-driven water oxidation, we propose that water oxidation catalysts may act similarly to P450's "compound I," a high-valent ferryl heme species. As the reactive intermediate in P450-mediated hydroxylation of hydrocarbons, compound I ("Fe(V)=O") is probably best described as S^{+}-Fe(IV)=O, where S^{+} is a cysteine sulfur cation radical. Oxidation by P450 proceeds by the "rebound" mechanism (Figure 5.8), wherein compound I abstracts hydrogen from the substrate, which is subsequently hydroxylated by OH• transfer from the iron center. Both ferrate and the putative Compound I feature a $^{3}A_{2}$ electronic

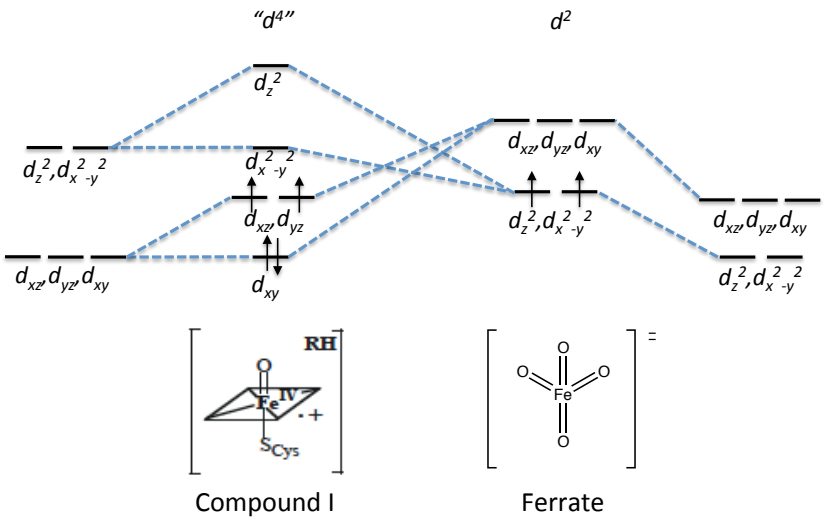

Figure 5.9. Simplified molecular orbital (MO) diagrams for the ferryl heme in Compound I of P450 (left) and FeO_4^{2-} (right).

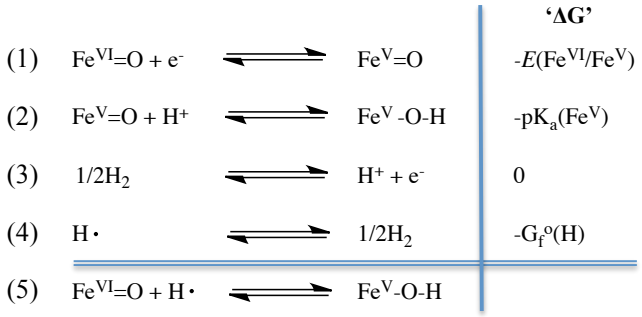

Figure 5.10. Thermodynamic cycle for determining *D*(O-H) ($-\Delta H_5$). 'ΔG' column indicates thermodynamic parameter relating to the free energy of each reaction, without constant factors (*e.g.*, $\Delta G_1 = -FE$).

ground state (Figure 5.9), which leads us to believe that they may exhibit similar reactivity towards substrates.

Using the hydrogen atom extraction mechanism of P450 as a *model*, we can estimate the thermodynamics of the ferrate oxidation system. Mayer has proposed that the relative strength of the $M^{(n-1)+}$-O-H bond following hydrogen atom extraction is of central importance in determining C-H activation by a metal-oxo species (Figure 5.8).[54] If the O-H bond in the one-electron reduced metal species (*D*(O-H)) is stronger than the C-H bond being broken (*D*(C-H)), the reaction can take place thermodynamically. Of primary interest, then, is the estimation of the homolytic bond dissociation energy (BDE), *D*(O-H).

The value of *D*(O-H) is equal to $-\Delta H^o$ for reaction (5) in Figure 5.10, and the thermodynamic cycle in Figure 5 can be utilized to estimate its value from empirical (*e.g.* redox couples, pK_a values) or calculated (*e.g.* free energy of formation for the hydrogen atom) parameters. Bordwell et al. have proposed[55] Eqn. 1 as an estimate of *D*(O-H), based on the cycle in Figure 5.10:

$$D(\text{O-H})\ (\text{kcal/mol}) = 23.06*[E(\text{Fe(VI)/Fe(V)})] + 1.37*pK_a(\text{Fe(V)}) + C, \qquad \text{(Eqn. 1)}$$

where C is the sum of the free energy of formation of the hydrogen atom (48.6 kcal/mol) and an 8.2-kcal $T\Delta S^o$ term. Eqn. 1 gives excellent (often ±1 kcal/mol) agreement with a multitude of literature values, and has been used by Green et al. to successfully estimate *D*(O-H) in chloroperoxidases.[56] Taking into account the increased reduction potential of ferrate versus permanganate (the calculated value of 2.20 V *vs*. NHE), and assuming that the pK_a of the

iron(V) species is similar to that of the iron(VI) species (pKa ~ 7.2),[50] *D*(O-H) = 117 kcal/mol under acidic conditions. This is clearly large enough to activate the strongest C-H bonds. Furthermore, this correctly predicts that ferrate is reactive enough to homolyze the O-H bond in water (~111 kcal/mol).

Holm and Donahue have tabulated a comprehensive series of oxo-transfer half reactions,

$$X_{(g)} + \tfrac{1}{2}O_{2(g)} \rightleftharpoons XO_{(g)}, \qquad \Delta H_{X/XO}\,(\text{kcal/mol})$$

which together can be used to determine the thermodynamic driving force for an oxygen atom transfer to occur, much like a standard reduction potential table.[57] Although not fully reproduced herein, it is interesting to note that (in the gas phase) OsO_4, a popular organic oxidant in spite of its high toxicity, features $\Delta H_{X/XO}$ = -12.8 kcal/mol, and is unable to effect oxygen atom transfer to water or chlorine (25.2 and 19.2 kcal/mol, respectively). We note, however, that ferrate *does* perform oxygen atom transfer to water, further indicating its strength relative to traditional oxidizing agents and allowing us to estimate its position on Holm's tables. The only substrate on the tables less susceptible to oxygen atom transfer is oxygen itself, with the production of ozone at $\Delta H_{X/XO}$ = +34.1 kcal/mol.

5.3.3. Water Oxidation Catalysts

Layered double hydroxides (LDHs), have been shown to be highly active for water oxidation.[58] We recently reported a well-defined [NiFe]-LDH nanomaterial (Figure 5.11) synthesized by pulsed laser ablation in liquids (PLAL).

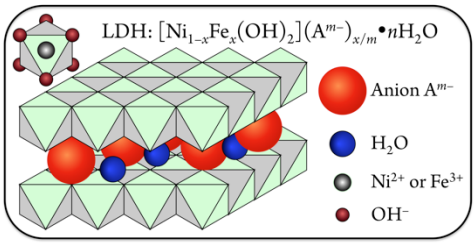

Figure 5.11. Structure of [NiFe]-LDH.

The scalable synthesis uses earth-abundant precursors and the prepared catalyst is isolated by simple centrifugation. Incorporating small amounts of titanium and lanthanum ions at the ppm level yields a material which is among the best water oxidation catalysts made of earth abundant elements ever reported.[59]

While the [NiFe]-LDH system is difficult to study *in situ* in aqueous environments due to its high water oxidation activity, it has been found that changing the solvent to a robust organic solvent (e.g. nitromethane or acetonitrile) permits the sequential generation of a variety of metastable species by increasing the applied potential to the electrode. Spectroscopic characterization of these intermediates has suggested the formation of an iron(VI) *cis*-dioxo species, similar in structure to a trapped ferrate. The proposed catalytic cycle, consistent with experimental findings, is shown in Figure 5.12. Application of a mild (~0.5 V vs NHE) potential oxidizes Ni(II) sites in the precatalyst cluster **I** to Ni(III) sites in the catalytically-relevant species **II**. Further oxidation of this cluster at a potential of ~0.6 V oxidizes the terminal and edge iron sites to Fe(IV) (species **III**). Potentials over 0.7 V generate species **IV** with ferrate-like terminal Fe(VI) centers at corner sites that are able to drop coordination number. This intermediate can then rearrange to **V**, a side-bound Fe(IV)-peroxide which liberates dioxygen upon binding of hydroxide.

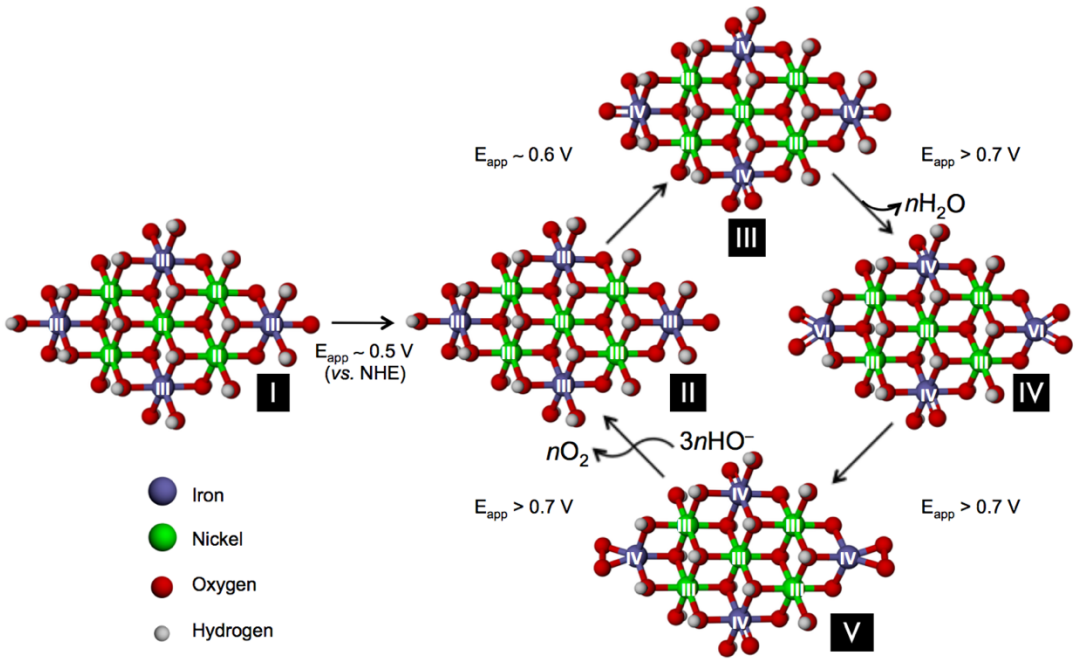

Figure 5.12. Proposed electocatalytic cycle for water oxidation with [NiFe]-LDH in base.

Spectroscopic studies of intermediates **IV** and **V** and the strategic injection of substrate water have verified the existence of a "trapped" ferrate species (Figure 5.12). Application of a +2.3 V (vs Pt in acetonitrile) potential in acetonitrile produces new infrared peaks centered at 856 and 877 cm^{-1}, consistent with a high-valent metal *cis*-dioxo motif. Addition of water to this electro-generated species results in the rapid bleaching of these features with the concomitant evolution of dioxygen. Furthermore, carrying out an extended electrolysis in the presence of $H_2{}^{18}O$ results in a characteristic shifting of these IR bands toward lower energy, providing strong evidence for 1) their correspondence to metal-oxo vibrational modes and 2) their relevance to catalysis.

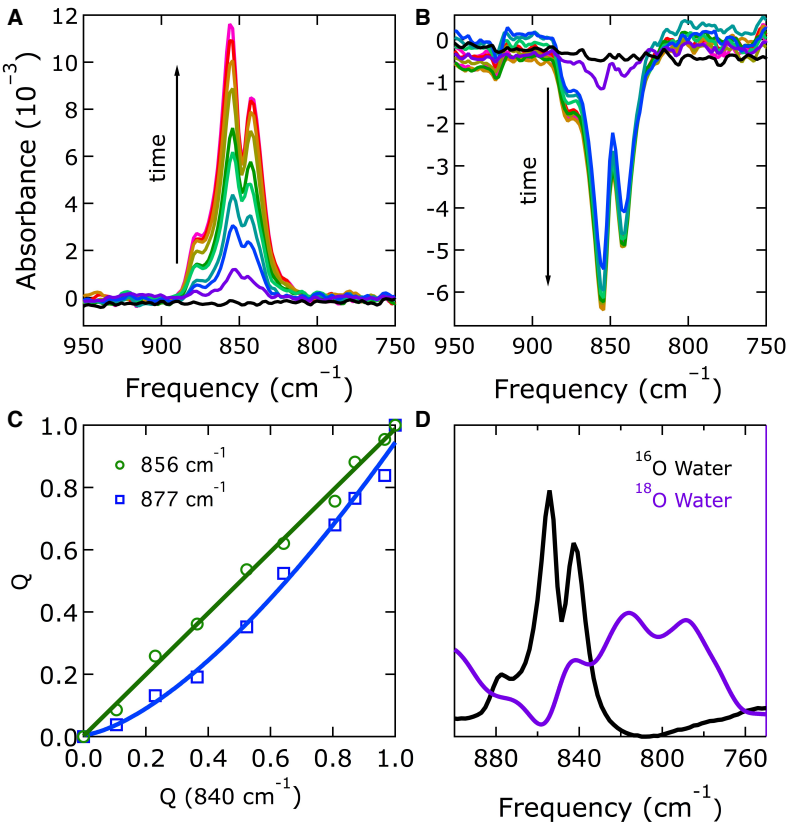

Figure 5.13. Spectroscopic evidence for the proposed intermediates. See Chapter 4.

Thus, our work suggests that the active site for water oxidation in [NiFe]-LDH nanosheets is a high-valent iron center resembling the ferrate anion (FeO_4^{2-}). The reactivity of ferrate is similar to that of permanganate,[38,39,41] with limited over-oxidation.[40] Unlike permanganate, ferrate is a poor epoxidation agent, producing instead allylic alcohols and cleaved products.[42] Taking into account the calculated reduction potential of ferrate (2.20 V *vs*. NHE), and assuming that the pK_a of the reduced Fe^{V} species is higher than that of Fe^{VI} (pKa ~ 7.2)[50], one can estimate that ferrate could activate C-H bonds as strong as 117 kcal/mol.

5.4. Methods and Materials

Standard oxidation reactions are performed in 0.1 M lithium perchlorate in acetonitrile or nitromethane with varying amounts of water (micromolar to millimolar in concentration).

The working electrode is prepared by drop-casting 120 uL of a 1mg/1mL catalyst suspension in water onto a fluorine-doped tin oxide (FTO) glass substrate. A typical three-electrode electrochemical cell is used with a platinum wire counter electrode and a silver/silver ion non-aqueous reference electrode.

Cyclic voltammetry is performed on blank FTO and catalyst-coated FTO, before and after the addition of substrate (millimolar concentration). Bulk electrolysis at a constant potential is used to generate products, which are detected by NMR (using solvent-suppression techniques) and gas chromatography coupled to mass spectrometry.

5.5. Results

5.5.1. Product Distributions for "Simple" Oxidations

We have shown that toluene oxidation in acetonitrile to benzaldehyde and benzyl alcohol is potential- and time-dependent (Figure 5.14). Of particular interest, no benzoic acid is detected.

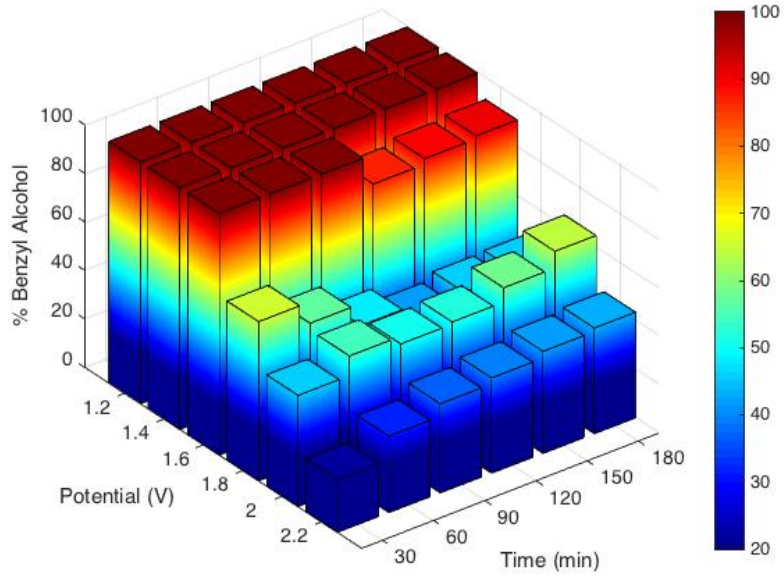

Figure 5.14. Product distribution (% benzyl alcohol relative to total benzyl alcohol and benzaldehyde produced) for [NiFe]-LDH electrolysis at various potentials and electrolysis times.

These studies, along with those involving other substrates, can be used to map the product distribution as a function of potential and electrolysis time. These "product landscapes" will serve as a roadmap for C-H activation of all types and strengths, with the goal of dialing-in a potential to obtain a desired distribution.

Other factors likely to affect product distribution are reaction (solvent) temperature, solvent composition (e.g. acetonitrile, nitromethane, etc.), catalyst loading, and substrate concentration. At low substrate concentration, for example, side reactions with solvent molecules have also been observed, leading to alternate products. These variables allow for further tuning of the system.

5.5.2. Functional Group Tolerance for "Complex" Transformations

Controlled methods to oxidize alkanes at room temperature are currently very limited and often result in over-oxidation to CO_2 and other undesired byproducts. The production of methanol from methane is a case in point. The mild oxidizing conditions employed in this system can be leveraged to favor specific products (Figure 5.15).

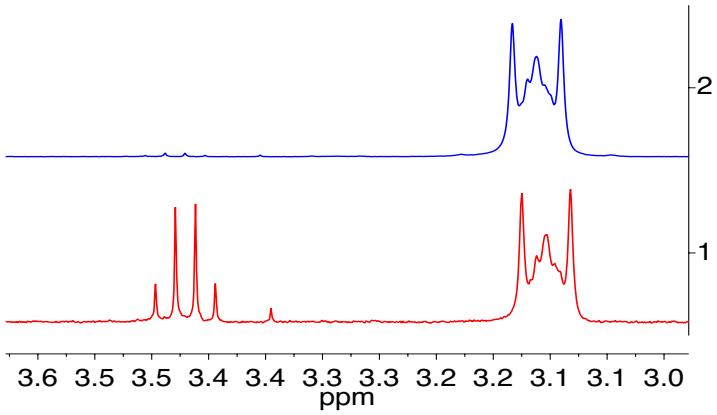

Figure 5.15. NMR spectra showing cyclohexane after bulk electrolysis (2 hours) without (top) and with (bottom) catalyst at 1.7 V vs. Ag/Ag^+ in 0.1 M $LiClO_4$ in acetonitrile. The peak at ~ 3.45 ppm corresponds to cyclohexanol. Spectra were scaled to the peak at 3.1 ppm, which is present in the electrolyte solution.

The production of allylic alcohols and ketones, important building blocks in the synthesis of organic compounds including pharmaceuticals, represents a significant challenge due to the propensity of the neighboring C=C double bond to undergo epoxidation. Preliminary data show that the double bond remains intact during oxidation for some substrates (Figure 5.16).

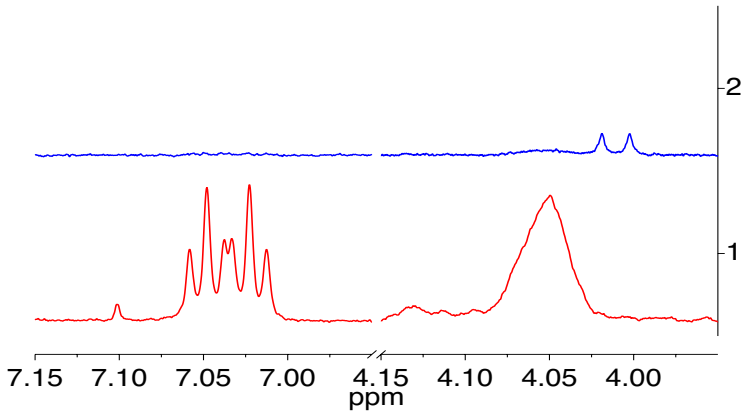

Figure 5.16. NMR spectra showing cyclohexene after bulk electrolysis (2 hours) without (top) and with (bottom) catalyst at 1.8 V vs. Ag/Ag^+ in 0.1 M $LiClO_4$ in acetonitrile. The peak at ~ 7.05 ppm corresponds to cyclohexen-one, while the peak at ~ 4.05 ppm corresponds to cyclohexen-ol.

Functional group tolerance may extend to alkynes, alcohols, ethers, epoxides, haloalkanes, aldehydes, ketones, esters, carboxylic acids, amides, amines, nitriles, imines, isocyanates, thiols, azos, and arenes.

5.5.3. Flow-Through Device for Rapid Conversion

A flow-through electrochemical device has been developed in which the flow rate and potential are easily controllable. Substrate enters the electrochemical cell through one port and product mixtures exit through a secondary port (Figure 5.17). Once the device is assembled, counter compartment (A) is filled with electrolyte solution through a port in the Teflon base. The counter electrode is a platinum wire (seen in A) fed through the Teflon base

in electrical isolation from the rest of the device. The counter compartment is separated from the working compartment by a Teflon disc fitted with a fine glass frit (B). A thin platinum wire is inlaid around the inner diameter of the Teflon disc and leaves the cell through a slot in (A) that has been coated to be nonconductive. This serves as the reference electrode. A thin (ca. 100 um) Teflon spacer (C) is sandwiched between (B) and the working electrode assembly (D), which holds the catalyst-coated FTO glass. Holes in the working electrode assembly (D) line up with the ports in (E). The threaded ring (F) screws on to (A) and is tightened to prevent leaking. Gaskets or O-rings between (A)/(B) and (D)/(E) prevent leaking. A predetermined potential is applied and substrate is pumped into one of the ports in (E), either by syringe or by peristaltic pump. In this way, substrate passes over the electrode without mixing with the electrolyte solution in the counter compartment, below. The high surface area of the electrode combined with the small volume inside the cell increases the current density and yield for a given flow rate.

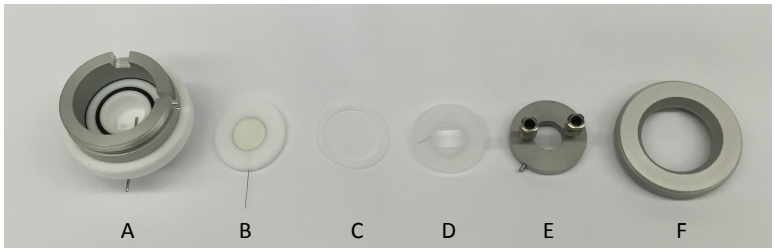

Figure 5.17. Flow-through cell (exploded view).

Figure 5.18. Assembled flow-through cell.

5.6. Future Directions

5.6.1. Specific Aims

The future of this project focuses on developing the [NiFe]-LDH water oxidation catalyst framework into an electrocatalytic hydrocarbon C-H oxidation system by exploiting the "trapped" ferrate sites present upon anodization. Simultaneously, other systems containing zeolite matrices supporting single-site ferrate anions will be designed. There are three specific aims proposed to accomplish these goals. First, accurate thermodynamic parameters must be measured *electrochemically*, both the proposed "trapped" systems and in solution. Specifically, we aim to measure E^{o}(Fe(VI/V)) in addition to observing higher oxidation states (*e.g.* Fe(VII) and Fe(VIII)). A detailed understanding of the thermodynamics of the system will help to design novel frameworks for oxidizing specific substrates, given the measured driving force. The second aim is to determine the scope of C-H electro-oxidation in "trapped" systems. The third aim is a mechanistic investigation of the viable electrocatalytic systems, with the goal of targeted improvement.

5.6.2. Aim 1: Electrochemical Measurement of Thermodynamic Properties

The electrochemistry of potassium ferrate is complicated by several factors: (1) it has limited solubility in traditional solvents; (2) its redox couple(s) are outside of the solvent window for most solvents; and (3) based on the increased oxidizing ability of Fe(V) and the terminal production of Fe(III) species, there is unlikely to be an observable, one-electron Fe(VI/V) couple.

Room temperature ionic liquids (RTILs) were developed specifically to have large electrochemical solvent windows, typically in excess of 5 V.[60] As such, they offer a significant improvement over common aqueous and organic electrolyte systems, such as tetrabutylammonium perchlorate in acetonitrile.[61] Additionally, the solubility of potassium ferrate may be improved in RTILs, such as trihexyl(tetradecyl)phosphonium bis-2,4,4-(trimethylpentyl)phosphinate (CYPHOS 104 IL). Preliminary experiments suggest that

K_2FeO_4 is somewhat soluble in propylene carbonate (PC) in the presence of the cryptand 4,7,13,16,21,24-hexaoxa-1,10-diazabicyclo[8.8.8]hexacosane, which has specificity for K^+ ions. Dry PC, frequently used in lithium-ion batteries, is reported to be stable up to 5 V *vs*. Li/Li^+.[62] Either of these solvent systems may be adequate for preliminary electrochemical investigations.

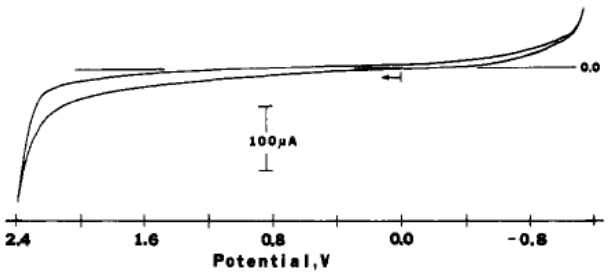

Figure 5.19. Cyclic voltammetric scan of the background at a platinum disk working electrode in 0.15 M tetrabutylammonium perchlorate-liquid sulfur dioxide at -40°C, showing typical anodic and cathodic potential limits. Reproduced from Ref. 63.

It is proposed that additional electrochemical studies are to be carried out in liquid sulfur dioxide. Tinker and Bard have reported[63] the benefits of experimentation in liquid SO_2, an aprotic, dipolar solvent with a large solvent window (Figure 5.19). Although relatively few studies involving liquid sulfur dioxide have been reported, early work demonstrated its utility in the electrolysis of various inorganic salts.[64] We are particularly interested in using SO_2 to access ferrate at higher oxidation states, potentially Fe(VII) and Fe(VIII). A gas at room temperature, isolation of electrolysis products from SO_2 is made simple by boiling off the solvent, though it should be noted that the presence of electrolyte introduces minor complications. Isolating high-valent iron species in this way would be very novel in itself, allowing for spectroscopic (*e.g.* EPR, Mössbauer) and mechanistic studies.

There are several potential challenges associated with the proposed electrochemical studies, primarily due to the fact that the one-electron redox couple may not be determinable. Since the Fe(V/IV) couple is likely to be more positive than the Fe(VI/V) couple under some conditions, ferrate may instead undergo a two-electron reduction; in this case, the simple "rebound" mechanism (*vide supra*) may be inadequate to describe the observed reactivity.

This scenario is highly dependent on the kinetics of the Fe(V) reduction or disproportionation, however, and the radical mechanism may still be operative for a two-electron oxidant. Furthermore, we predict that ferrate will be an excellent oxo-transfer agent, which may react directly with the liquid SO_2, forming SO_3. Holm's thermodynamic tables (*vide supra*) indicate that this reactivity is viable.

A possible solution to these issues is to utilize a *zeolitic framework for electrochemical measurements*. There is little precedent for extensive electrochemical studies on guest molecules embedded in zeolites, although at least one study has examined their semi-conductor nature.[65] Other groups have successfully synthesized "silver-exchanged" zeolites, in which some or all of the supporting cations are replaced by Ag^+.[66] Chronopotentiometric measurements, carried out in powdered graphite, show reversible reduction and oxidation of the silver guest ions, inferring electrical conductivity with the electrode. We propose screening of a variety of solvents, including RTILs, PC, and liquid SO_2, at a carbon-paste electrode with 50% zeolite by weight. Within the zeolite pores, higher *and* lower iron oxidation states may be stabilized, similar to the stabilizing effects of heme protein domains, possibly allowing for the isolation of the one-electron oxidized and reduced ferrate. These species are likely unstable in solution due to the formation of μ-oxo dimers.

A method for supporting potassium ferrate in a zeolite scaffold structure will be modified from that reported for potassium permanganate in Y- and β-Zeolite.[45,46] Zeolite pellets of various sizes, porosity, and structures will be added to aqueous, basic solutions of potassium ferrate and allowed to incorporate. The water will subsequently be removed from the reaction mixture under reduced pressure, and non-adsorbed potassium ferrate will be physically separated by a mesh screen. The resulting ferrate-on-zeolite material will be mixed with varying amounts of graphite (or graphite paste) to produce active catalyst that can be pressed into columns or cartridges.

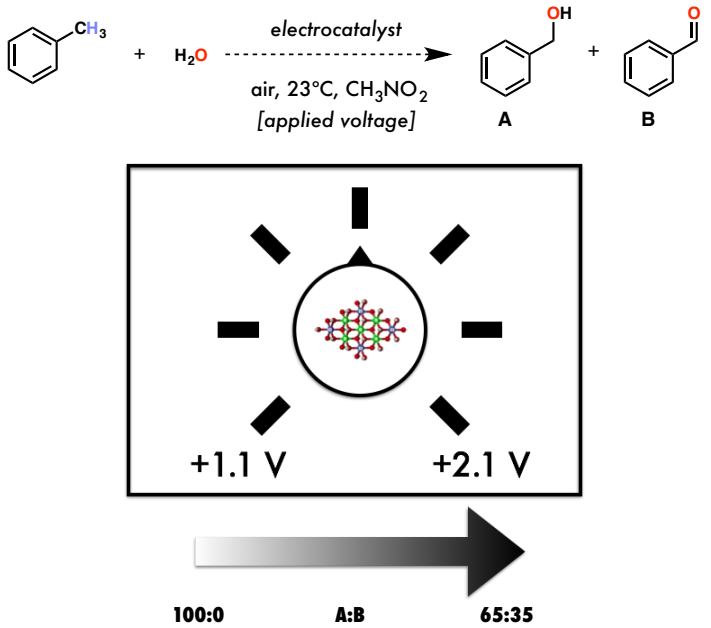

Figure 5.20. The selectivity of C–H electro-oxidation of toluene using the [NiFe]-LDH catalyst can be tuned by modulating the applied potential in nitromethane (or acetonitrile). Figure reproduced with permission from Julian West.

5.6.3. Aim 2: Scope of C-H Electro-Oxidation

Initial experiments show the [NiFe]-LDH catalyst to be highly active for the selective oxidation of simple hydrocarbons. Starting with toluene, the PCET products benzyl alcohol and benzaldehyde are produced, and the distribution can be tuned by modulating the applied potential. At low potentials (< 1.1 V vs Ag^{+}/Ag in nitromethane) only benzyl alcohol is formed, while at high (ca. 2.1 V vs Ag^{+}/Ag) potentials both benzyl alcohol and benzaldehyde are formed in a 2:1 ratio (Figure 5.20). Under all conditions no benzoic acid is formed. To the best of our knowledge, this constitutes the first example of an electrochemically tunable C–H oxidation catalyst.

Further study using cyclohexene as a substrate has shown cyclohexen-3-ol and cyclohexenone to be the sole organic oxidation products, again suggesting a NOCHA process (Figure 5.21). Interestingly, cyclohexene oxide is not formed under these conditions, a sharp

departure from many other high-valent metal-oxo systems (though common for ferrate oxidation chemistry).

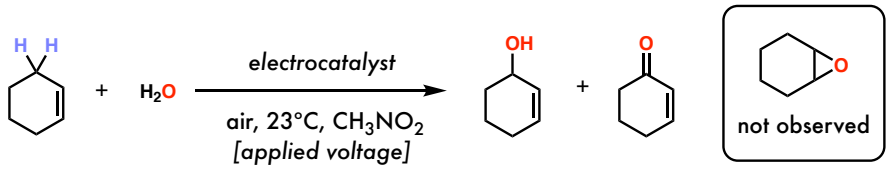

Figure 5.21. Cyclohexene is cleanly oxidized to cyclohexen-3-ol and cyclohexanone under the electrocatalytic conditions. No cyclohexene oxide is detected. Figure reproduced with permission from Julian West.

A final highly-relevant preliminary result was found in the selective oxidation of methane to methanol when the reaction was carried out in nitromethane as a solvent. This reaction has been a longstanding grand challenge in organometallic chemistry and has particular relevance to the energy security of the United States in light of the current shale gas boom.[67] We plan to further investigate and optimize the efficiency of this oxidation and those of other simple hydrocarbons, with the study proceeding in three phases of increasing complexity.

Phase I: Oxidation of simple saturated and unsaturated hydrocarbons

We plan to optimize the reaction conditions (solvent, time, potential, temperature, etc.) for the aforementioned examples and extend them to other simple hydrocarbons. We aim to include linear, branched, cyclic, and polycyclic hydrocarbons in the initial studies (Figure 5.22). Product determination will be accomplished primarily using NMR and gas chromatography (FID and MS coupled) techniques.

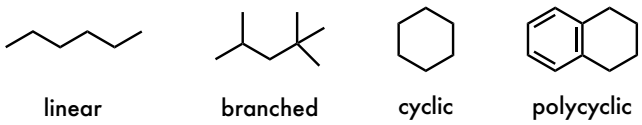

Figure 5.22. Examples of hydrocarbons for study in Phase I. Figure reproduced with permission by Julian West.

Simultaneous to our studies with [NiFe]-LDH, we propose testing the catalytic efficiency of zeolite-encapsulated ferrate. Before attempting electrocatalytic oxidation cycles, we plan to begin with stoichiometric oxidations, similar to the potassium permanganate work described above. These experiments will allow for proper screening of solvent, zeolite, and time conditions for maximum substrate turnover. Because the zeolite structure plays an important role in permanganate reactivity, we expect similar sensitivity with the ferrate system. It is also critical to determine experimental conditions that will limit the amount of ferrate that leaches out of the zeolite framework. Both oxidation conditions and adsorption techniques can be developed to minimize desorption. Finally, stoichiometric studies will determine the scope of the reaction, identifying which substrates can be successfully oxidized by the system at the reaction conditions.

Once optimal conditions have been established, oxidations will be carried out by forcing substrate solutions through activated cartridges of zeolite material by means of a pump or syringes. The ratio of graphite (for support and electrical conductivity) to zeolite material (for catalysis) will be modulated to ensure that solutions can flow freely through the columns while still retaining their structural stability. Solutions exiting the cartridge will be collected and solvent will be removed by evaporation. Products will be analyzed by conventional means (*e.g.*, NMR, GC/MS). Desorption of ferrate from the zeolite will be tested by UV-visible absorption spectroscopy of column washes.

The novelty of this system is ultimately based on the catalytic, reusable nature of the ferrate columns. There are two possible recharging cycles that are proposed here (Figure 5.23): (1) direct electro-regeneration of ferrate from the nominally iron(III) decomposition species or (2) reduction of the iron(III) species to iron(0), followed by a secondary oxidation to ferrate(VI) *in situ*. In early work, regeneration will be performed in standard, 3-component electrochemical cells.

Cycle I depends on the direct oxidation of iron(III) oxides (rust) to ferrate at the anode. Preliminary electrochemical synthesis experiments indicate that this is not a straightforward task; because the iron(III) products dimerize and form μ-oxo species in aqueous solution, the mononuclear iron(VI) product is not observed. Cycle I may remain a

feasible model, however, because the iron(III) oxides will be immobilized inside the pores of the zeolite, preventing aggregation and the formation of bridging oxos.

In Cycle II, the Fe_2O_3 is initially reduced to iron metal (there is precedent for electrochemical reduction of rust to Fe_3O_4)[68] inside the zeolite pores. Although the lattice structure of iron rust generally prevents its direct reduction to Fe(0), the unique environment

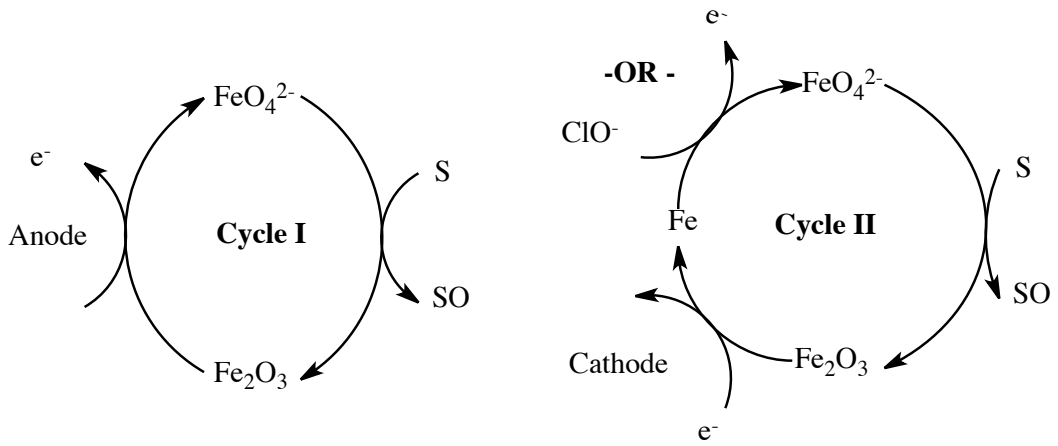

Figure 5.23. Two possible electrocatalytic cycles for zeolite supported ferrate cartridges. In Cycle I (left), the iron(III) decay product is directly re-oxidized to ferrate at the anode after substrate has been oxidized (S → SO). In Cycle II, the iron(III) decay product is first reduced to iron(0) at the cathode before being oxidized back to ferrate. Cycle II requires electrochemical "pulsing" of the electrode. In Cycle II, the second oxidation step could be performed chemically by hypochlorite.

of the zeolite pores may again prove useful here. Following a cathodic sweep, the electrode will be poised anodically, regenerating ferrate. The electrochemical synthesis of ferrate from Fe(0) has been accomplished as a preliminary result.

The regeneration of ferrate *in situ* may prove challenging electrochemically due to the high potentials that are needed. Specifically, the graphite/carbon paste would need to be robust at such high potentials. One alternative method is shown in Cycle II of Figure 5.23, where the wet chemical synthesis (*i.e.* bleach method, *vide supra*) is utilized instead of the direct oxidation at the electrode.

Following initial studies, our goal is to develop a continuous-flow electrocatalytic cartridge for organic oxidations. Although the mechanism is identical to that detailed above,

significant mechanical engineering would need to take place to ensure that organic substrates are not present in the cell when cartridge regeneration occurs. A pump valve, interfaced with the voltage source, could force substrate out of the column with aqueous base to prepare for regeneration. Following regeneration of the packing material, another valve could dispose of (or recycle) the aqueous waste, clearing the column for refilling with organic substrate. An automated system as described could find use in industry for large-scale oxidations.

For the [NiFe]-LDH material, which can be immobilized on conductive glass, a prototype flow-through device has been designed and built (Figure 5.24.). The device, which features a 100μm substrate channel, is intended to oxidize substrate as it passes over the anodized catalyst layer. We plan to work with industry partners to scale this device up to medium- and large-scale reactions.

Figure 5.24. Flow-through cell.

Phase II: Oxidation of mixtures of hydrocarbons

While selective oxidation of a single substrate is itself useful, the capacity of the catalyst to distinguish between similar components in a complex mixture for selective oxidation could also be of high interest. We propose reacting mixtures of the previously studied hydrocarbons and assaying the proportion of oxidized products. An example is provided in Figure 5.25.

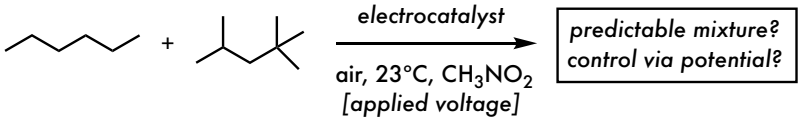

Figure 5.25. An example competition experiment for the oxidation of two hydrocarbons, as proposed in Phase II. Figure reproduced with permission by Julian West.

Phase III: Oxidation of partially oxidized hydrocarbons

The controlled oxidation of partially oxidized hydrocarbons while avoiding mineralization could be synthetically valuable, particularly true if secondary oxidation occurs predictably in response to the existing oxidation (whether through electronic effects or directivity). Additionally, the existing C–H oxidation literature[15,18,22] typically involves this substrate class, allowing us to compare and contrast our method using substrates such as in Figure 5.26; these are the substrates generally targeted by the pharmaceutical industry.

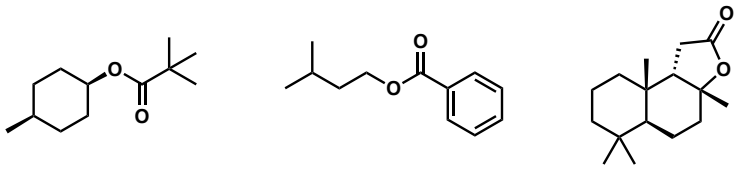

Figure 5.26. Example of partially oxidized hydrocarbons to be studied during Phase III. Figure reproduced with permission by Julian West.

5.6.4. Aim 3: Mechanistic Investigation

We will build on our synthetic observations with mechanistic insight to better understand and improve our oxidation system. Toluene is oxidized only to benzyl alcohol at low potentials with benzaldehyde becoming accessible at high potentials. The spectroscopic studies suggest that this divergent reaction outcome results from the formation of different oxidizing species under the electrocatalytic conditions, with an Fe(IV) terminal oxo site proposed for oxidations at low potentials and an Fe(VI) ferrate-like terminal site emerging under high potentials. We propose to use these same techniques to assay the speciation of the catalyst under relevant C–H oxidation conditions and interrogate this hypothesis.

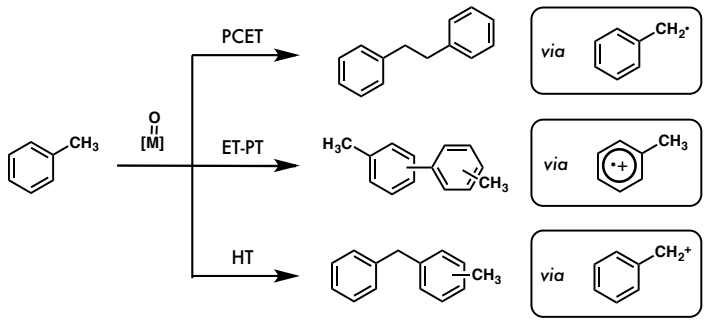

Figure 5.27. Differentiated products from the oxidation of toluene by metal-oxo catalysts, with bibenzyl, biaryl, and diarylmethane implicating PCET, ET-PT, and HT, respectively. Figure reproduced with permission by Julian West.

We also aim to determine which NOCHA mechanism(s) is(are) operative: ET-PT, PCET, or HT. Seminal studies by Mayer[69] on metal-oxo C–H oxidations have revealed that the oxidation of toluene, a compatible substrate with this method can provide characteristic side products depending on mechanism, with biphenyl (PCET/HAT), biaryl (ET-PT), and diarylmethane (HT) being highly suggestive of some mechanistic contribution from each possibility (Figure 5.27). KIE results can also help distinguish between PCET and ET-PT oxidations of alkanes. Concerted O-atom insertion and OH^+ insertion can be elucidated by the judicious use of stereochemical and radical clock probes. Together, these results could help inform what other synthetic applications would be most effective to target with this C–H activation electocatalyst. Additionally, we will pursue experiments to test for the presence of Fenton-type reaction pathways.

5.7. Conclusion

The development of a "green," sustainable, and selective hydrocarbon oxidation catalyst would be of great importance. It is proposed to utilize a high-performing, earth-abundant water oxidation catalyst to drive a robust, heterogeneous electrocatalytic system based on the immobilized ferrate anion (FeO_4^{2-}). The primary goal will be assaying and tuning the selectivity of this reaction for a variety of hydrocarbon feedstocks, a pursuit will be informed by concurrent mechanistic study. This experience and understanding will then allow us to

extend this approach to the development of new, useful C–H functionalization reactions of hydrocarbons, with C–H fluorination being our starting point.

5.8. References and Notes

(1) Arndtsen, B. A.; Bergman, R. G.; Mobley, T. A.; Peterson, T. H. *Acc. Chem. Res.* **1995**, *28*, 154.

(2) Shilov, A. E.; Shul'pin, G. B. *Chem. Rev.* **1997**, *97*, 2879.

(3) Labinger, J. A.; Bercaw, J. E. *Nature* **2002**, *417*, 507.

(4) Yu, J.-Q. *Adv. Synth. Catal.* **2014**, *356*, 1393.

(5) Godula, K.; Sames, D. *Science* **2006**, *312*, 67.

(6) Gutekunst, W. R.; Baran, P. S. *Chem. Soc. Rev.* **2011**, *40*, 1976.

(7) Goldshleger, N.; Tyabin, M.; Shilov, A.; Shteinman, A. *Russian Journal of Physical Chemistry* **1969**, *43*, 1222.

(8) Janowicz, A. H.; Bergman, R. G. *J. Am. Chem. Soc.* **1982**, *104*, 352.

(9) Hoyano, J. K.; Graham, W. A. *J. Am. Chem. Soc.* **1982**, *104*, 3723.

(10) Waterman, R. *Organometallics* **2013**, *32*, 7249.

(11) Mayer, J. M.; Larsen, A. S.; Bryant, J. R.; Wang, K.; Lockwood, M.; Rice, G.; Won, T.-J.; ACS Publications: 2004.

(12) Yan, M.; Lo, J. C.; Edwards, J. T.; Baran, P. S. *J. Am. Chem. Soc.* **2016**, *138*, 12692.

(13) Que, L.; Tolman, W. B. *Nature* **2008**, *455*, 333.

(14) Shilov, A. E.; Shteinman, A. A. *Acc. Chem. Res.* **1999**, *32*, 763.

(15) Groves, J. T.; Nemo, T. E. *J. Am. Chem. Soc.* **1983**, *105*, 6243.

(16) Barona-Castaño, J. C.; Carmona-Vargas, C. C.; Brocksom, T. J.; de Oliveira, K. T. *Molecules* **2016**, *21*, 310.

(17) Que Jr, L. *Acc. Chem. Res.* **2007**, *40*, 493.

(18) Chen, M. S.; White, M. C. *Science* **2007**, *318*, 783.

(19) Bigi, M. A.; Reed, S. A.; White, M. C. *Nat. Chem.* **2011**, *3*, 216.

(20) *Oxidation in Organic Chemistry: Part A*; Wiberg, K. B., Ed.; Academic Press: New York, 1965.

(21) Joglekar, M.; Nguyen, V.; Pylypenko, S.; Ngo, C.; Li, Q.; O'Reilly, M. E.; Gray, T. S.; Hubbard, W. A.; Gunnoe, T. B.; Herring, A. M. *J. Am. Chem. Soc.* **2015**, *138*, 116.

(22) Horn, E. J.; Rosen, B. R.; Chen, Y.; Tang, J.; Chen, K.; Eastgate, M. D.; Baran, P. S. *Nature* **2016**.

(23) Reidies, A. H. In *Ullmann's Encyclopedia of Industrial Chemicals*; Wiley-VCH: Weinheim, 2002.

(24) Hoppe, M. L.; Schlemper, E. O.; Murmann, R. K. *Acta Crystallogr.* **1982**, *B38*, 2237.

(25) Ockerman, L. T.; Schreyer, J. M. *J. Am. Chem. Soc.* **1951**, *73*, 5478.

(26) Thompson, G. W.; Ockerman, L. T.; Schreyer, J. M. *J. Am. Chem. Soc.* **1951**, *73*, 1379.

(27) Sharma, V. K.; O'Brian, B.; Smith, J. O. *J. Am. Chem. Soc.* **1997**, *213*, 238.

(28) Carr, J. D. In *Ferrates*; Sharma, V. K., Ed.; American Chemical Society: 2008; Vol. 985, p 189.

(29) Hrostowski, H. J.; Scott, A. B. *J. Chem. Phys.* **1950**, *18*, 105.

(30) Caddick, S.; Murtagh, L.; Weaving, R. *Tetrahedron* **2000**, *56*, 9365.

(31) Macova, Z.; Bouzek, K.; Hives, J.; Sharma, V. K.; Terryn, R. J.; Baum, J. C. *Electrochimica Acta* **2009**, *54*, 2673.

(32) Lapique, F.; Valentin, G. *Electrochem. Comm.* **2002**, *4*, 764.

(33) He, W.; Wang, J.; Shao, H.; Zhang, J.; Cao, C. *Electrochem. Comm.* **2005**, *7*, 607.

(34) Herren, M.; Güdel, H. U. *Inorg. Chem.* **1992**, *31*, 3683.

(35) Brunold, T. C.; Hauser, A.; Güdel, H. U. *J. Lumin.* **1994**, *59*, 321.

(36) Brunold, T. C.; Güdel, H. U.; Kuck, S.; Huber, G. *J. Lumin.* **1995**, *65*, 293.

(37) Wagner, W. F.; Gump, J. R.; Hart, E. N. *Anal. Chem.* **1952**, *24*, 1497.

(38) Audette, R. J.; Quail, J. W.; Smith, P. J. *Tet. Lett.* **1971**, *12*, 279.

(39) Bemiller, J. N.; Kumari, V. G.; Darling, S. D. *Tet. Lett.* **1972**, *36*, 4143.

(40) Tsuda, Y.; Nakajima, S. *Chem. Lett.* **1978**, *7*, 1397.

(41) Sharma, V. K.; Burnett, C. R.; Rivera, W.; Joshi, V. N. *Langmuir* **2001**, *17*, 4598.

(42) Ho, C.-M.; Lau, T.-C. *New J. Chem.* **2000**, *24*, 587.

(43) Wood, R. H. *J. Am. Chem. Soc.* **1957**, *80*, 2038.

(44) Delaude, L.; Laszlo, P. *J. Org. Chem.* **1996**, *61*, 6360.

(45) Regen, S. L.; Koteel, C. *J. Am. Chem. Soc.* **1977**, *99*, 3837.

(46) Quici, S.; Regen, S. L. *J. Org. Chem.* **1979**, *44*, 3436.

(47) Sreekumar, R.; Padmakumar, R. *Tet. Lett.* **1997**, *38*, 5143.

(48) Davis, M. E.; Lobo, R. F. *Chem. Mater.* **1992**, *4*, 756.

(49) Bielski, B. H. J.; Thomas, M. J. *J. Am. Chem. Soc.* **1987**, *109*, 7761.

(50) Rush, J. D.; Zhao, Z.; Bielski, B. H. J. *Free Rad. Res.* **1996**, *3*, 187.

(51) Rush, J. D.; Bielski, B. H. J. *Inorg. Chem.* **1989**, *28*, 3947.

(52) Sarma, R.; Angeles-Boza, A. M.; Brinkley, D. W.; Roth, J. P. *J. Am. Chem. Soc.* **2012**, *37*, 15371.

(53) Lee, D. G.; Gai, H. *Can. J. Chem.* **1993**, *71*, 1394.

(54) Mayer, J. M. *Acc. Chem. Res.* **1999**, *31*, 441.

(55) Bordwell, F. G.; Cheng, J.; Ji, G.; Satish, A. V.; Zhang, X. *J. Am. Chem. Soc.* **1991**, *113*, 9790.

(56) Green, M. T.; Dawson, J. H.; Gray, H. B. *Science* **2004**, *304*, 1653.

(57) Holm, R. H.; Donahue, J. P. *Polyhedron* **1993**, *12*, 571.

(58) Corrigan, D. A. *J. Electrochem. Soc.*, *132*, 377.

(59) Hunter, B. M.; Blakemore, J. D.; Deimund, M.; Gray, H. B.; Winkler, J. R.; Müller, A. M. *J. Am. Chem. Soc.* **2014**, *136*, 13118.

(60) Bonhote, P.; Dias, A.-P.; Papageorgiou, N.; Kalyanasudaram, K.; Graetzel, M. *Inorg. Chem.* **1996**, *35*, 1168.

(61) Mann, C. In *Electroanalytical Chemistry: A Series of Advances*; Bard, A. J., Ed.; Marcel Dekker: New York, 1969, p 57.

(62) Ossola, F.; Pistoia, G.; Seeber, R.; Ugo, P. *Electrochim. Acta* **1988**, *33*, 47.

(63) Tinker, L. A.; Bard, A. J. *J. Am. Chem. Soc.* **1978**, *101*, 2316.

(64) Bagster, L. S.; Steele, B. D. *Chem. News* **1912**, *105*, 157.

(65) Alvaro, M.; Cabeza, J. F.; Fabuel, D.; Garcia, H.; Guijarro, E.; Martinez de Juan, J. L. *Chem. Mater.* **2005**, *18*, 26.

(66) Pereira-Ramos, J.-P.; Messina, R.; Perichon, J. *J. Electroanal. Chem.* **1982**, *146*, 157.

(67) U.S. Energy Information Administration. Table 4.1 Technically Recoverable Crude Oil and Natural Gas Resource Estimates, 2009 https://www.eia.gov/totalenergy/data/annual/showtext.php?t=ptb0401 (accessed Jan 15, 2016).

(68) Suzuki, I.; Masuko, N.; Hisamatsu, Y. *Corrosion Science* **1979**, *19*, 521.

(69) Larsen, A. S.; Wang, K.; Lockwood, M. A.; Rice, G. L.; Won, T.-J.; Lovell, S.; Sadílek, M.; Tureček, F.; Mayer, J. M. *J. Am. Chem. Soc.* **2002**, *124*, 10112.